



**HAL**  
open science

# Study of a thermo-acoustic instability triggering in a low-swirl burner using simultaneous time-resolved acetone and OH-PLIF

Antoine Renaud, Takeshi Yokomori, Shigeru Tachibana

► **To cite this version:**

Antoine Renaud, Takeshi Yokomori, Shigeru Tachibana. Study of a thermo-acoustic instability triggering in a low-swirl burner using simultaneous time-resolved acetone and OH-PLIF. Proceedings of the Combustion Institute, 2019, 37, pp.2627 - 2633. 10.1016/j.proci.2018.08.036 . hal-03486385

**HAL Id: hal-03486385**

**<https://hal.science/hal-03486385>**

Submitted on 20 Dec 2021

**HAL** is a multi-disciplinary open access archive for the deposit and dissemination of scientific research documents, whether they are published or not. The documents may come from teaching and research institutions in France or abroad, or from public or private research centers.

L'archive ouverte pluridisciplinaire **HAL**, est destinée au dépôt et à la diffusion de documents scientifiques de niveau recherche, publiés ou non, émanant des établissements d'enseignement et de recherche français ou étrangers, des laboratoires publics ou privés.



Distributed under a Creative Commons Attribution - NonCommercial 4.0 International License

# Study of a thermo-acoustic instability triggering in a low-swirl burner using simultaneous time-resolved acetone and OH-PLIF.

Antoine Renaud<sup>a,\*</sup>, Takeshi Yokomori<sup>b</sup>, Shigeru Tachibana<sup>c</sup>

<sup>a</sup>Laboratoire EM2C, CNRS, CentraleSupélec

<sup>b</sup>Faculty of Science and Technology, Keio University

<sup>c</sup>Aeronautical Technology Directorate, Japan Aerospace Exploration Agency (JAXA)

---

## Abstract

A low-swirl burner operating in premixed mode with methane and air is studied using high-speed acetone and OH-PLIF and advanced post-processing methods. In a transient operating point where the equivalence ratio is slowly increased while keeping the bulk velocity constant, a thermo-acoustic instability is found to grow and generate large pressure fluctuations in the combustion chamber. The instability is maintained by bursts of flame in phase with the pressure fluctuation cycle. It is found that these bursts are amplified by the fact that the boundaries of the flame arms are fluctuating in phase. This phasing of the arms' boundaries is due to the change in flame speed coming from the increase of equivalence ratio.

### Keywords:

low swirl, time-resolved, DMD, Hilbert transform

---

## 1. Introduction

Lean premixed combustion is a widely acknowledged way to control nitrogen oxides emissions because it allows to control the combustion temperature and thus the production of thermal-NO<sub>x</sub> [1]. A main drawback of lean premixed flames is however their sensitivity to external perturbations and their propensity to trigger thermo-acoustic instabilities when used in confined conditions such as within the combustion chamber of a gas-turbine. Thermo-acoustic instabilities can generate high pressure fluctuation levels leading to the flame blow-off or damages to the burner [2].

In the present study, a low-swirl burner is used. This kind of injectors, first developed at the Lawrence Berkeley National Laboratory [3, 4], is known for its reduced pollutant emissions [5] and may therefore prove interesting for gas turbine applications. Low swirl injectors also present promising properties regarding fuel flexibility as they can easily accommodate several types of

gaseous fuels such as methane, hydrogen or syngas [6–8]. From a more fundamental point of view, low-swirl injectors create a divergent flow without any inner recirculation zone, thus allowing to stabilize a freely propagating planar turbulent flame around the center of the burner and have therefore been used in detailed turbulent combustion studies [9].

The dynamical behavior of confined low-swirl flames has been the subject of several experimental and numerical studies [10–16]. Therkelsen et al. [14] analyzed CH<sub>4</sub>-air and H<sub>2</sub>/CH<sub>4</sub>-air flames that presented self-sustained thermo-acoustic instabilities. Thanks to phase-locked PIV measurements, they highlighted ring vortices periodically detaching from the burner rim in the external shear layer as the main mechanism leading to the instability.

Laser diagnostics are a key tool in combustion studies because of their minimal intrusiveness [17]. High-speed Planar Laser-Induced Fluorescence (PLIF) gained momentum with the advances in high-speed dye lasers, image intensifiers and cameras and is now mature. This technique provides numerous advantages for the study of flame dynamics [18] and enables the use of well-established signal processing tools such as Fourier transform and its derivatives.

In the present study, as the equivalence ratio of

---

\*Corresponding author: Antoine RENAUD; Laboratoire EM2C, CNRS, CentraleSupélec; 3 rue Joliot Curie; 91190 Gif-sur-Yvette, France

Email address: [antoine.renaud@centralesupelec.fr](mailto:antoine.renaud@centralesupelec.fr)  
(Antoine Renaud)

a methane-air low-swirl flame in confined conditions is increased, the pressure fluctuations also grow because of the triggering of a thermo-acoustic instability. Using time-resolved laser-induced fluorescence diagnostics and advanced post-processing techniques, the growth of the instability is studied and is found to be linked to the increase in flame speed due to the increase of the equivalence ratio.

## 2. Experimental Methods

### 2.1. Experimental Setup

The setup used in this study is shown in Fig.1.

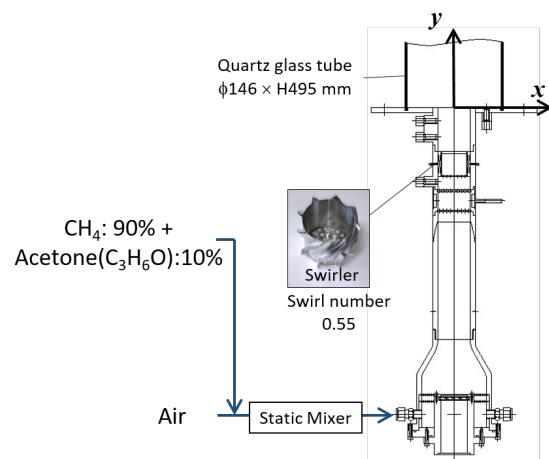


Figure 1: Schematics of the low-swirl burner.

The low-swirl burner uses a premixture of methane and air which is sent through a particular swirler, shown in a smaller picture in Fig.1. The outer part of the swirler has a swirl number of 0.55 to give the outer flow a rotational motion while the inner part has holes to let the mixture through. By effectively combining an axial injection and a swirl, this creates a divergent flow field in the combustion chamber without any recirculation zone. A turbulent flame can thus be stabilized aerodynamically. The exit diameter of the injector is 50 mm and the mixture flows in a 495 mm-long cylindrical combustion chamber (diameter: 146 mm) made of fused silica.

Because the behavior of the fresh gases is studied in the present work, 10% (in volume) of acetone is added to the fuel as a fluorescent tracer. This ratio is chosen to optimize the fluorescence signal without disturbing too much the combustion reaction [19].

To study the growth of a thermo-acoustic instability, a transient operating point is used. The bulk velocity at

the exit of the injector is kept constant at  $10 \text{ m.s}^{-1}$ . During the 4.4 second transient operation time, the equivalence ratio is progressively increased from 0.66 to 0.70. This results in a global power increase from 45 to 48 kW.

### 2.2. Diagnostics

To allow for the simultaneous imaging of both fresh and burnt gases, a dual high-speed acetone and OH PLIF setup is used. Since acetone is added to the fresh mixture and burns at the flame front, a fluorescence signal from acetone means that fresh gases are present. On the contrary, OH is produced at the flame front and remains in the post-flame zone where it will be slowly oxidized, meaning that the OH fluorescence signal represents the reaction products. To excite both species, a 283.6 nm wavelength generated by a dye laser operated on Rhodamine (Sirah Credo-DYE-Amp-SH-FE) is used. The dye laser is pumped by a 10 kHz Nd:YAG laser (Edgewave IS-400-2-L) and the pulse energy at the exit of the dye laser is 0.6 mJ. A 105 mm-high and 1 mm thick laser sheet is used to illuminate an axial-radial plane through the combustion chamber.

The fluorescence signal from acetone is recorded thanks to a NAC Memrecam HX-3 camera equipped with an image intensifier (Invisible Vision) and a 50 mm, f:1.8 lens with a short pass filter (525 nm). The resulting  $768 \times 512$  pixels picture corresponds to one half of the chamber diameter. To record the fluorescence from OH, a Photron Fastcam SA-X2 camera is used with a Lambert HiCATT image intensifier, a 45mm, f:1.8 UV lens and a 320/40 nm filter. The  $1024 \times 1024$  pixels image corresponds to the whole burner diameter. Both cameras record at 10,000 fps with a resolution of 0.135 mm/pixel and each camera records 43684 images, corresponding to a little less than 4.4 seconds. This duration corresponds to the size of the buffer memory of the cameras.

A pressure transducer (Kulite WCT-312-5SG) is placed at the dump wall of the combustion chamber and its signal is recorded at 200 kHz. Only the part during which the cameras are recording is shown in this study.

Because of the time-resolved nature of the diagnostics, specific post-processing methods are available and are described in the following.

### 2.3. Post-processing methods

Time-resolved data obtained from high-speed OH and acetone PLIF contain a lot of information but also some noise. In order to extract useful material, namely spatial structures or frequencies in the flame response, Dynamic Mode Decomposition (DMD) is used

in this study. DMD is a linear analysis technique which extracts monochromatic modes from a set of time-resolved data [20, 21]. This characteristic makes it very useful for analyzing thermo-acoustic oscillations since they generally offer a narrow frequency response.

DMD modes are complex-valued and depend on both spatial and temporal coordinates. A general form for a DMD mode can be given by the following expression

$$M(x, t) = K(x)e^{i\phi(x)}e^{(a+i\omega)t} = f_{space}(x)g_{time}(t) \quad (1)$$

where  $K(x)$  is a spatially dependent oscillation amplitude,  $\phi(x)$  represents a spatially dependent phase and  $e^{(a+i\omega)t}$  is the temporal content of the mode, which is a composition of an oscillation and an exponential envelope. In the present studies, the DMD modes that are studied are all steady and thus  $a$  is very small, meaning that the temporal part is a simple sinusoidal oscillation  $e^{i\omega t}$ . It is thus easy to separate the spatial content  $f_{space}$  from the temporal content  $g_{time}$  of the mode.

In the present study, time-resolved diagnostics are used to study a transient operating point. It is thus interesting to obtain instantaneous properties for a given signal and for this purpose, Hilbert transform is used. Given a temporal signal  $s(t)$ , the Hilbert transform is defined as:

$$H_s(t) = \frac{1}{\pi} \int_{-\infty}^{\infty} \frac{s(\tau)}{t - \tau} d\tau. \quad (2)$$

The main use of the Hilbert transform lies in the fact that it enables to compute the analytical signal  $s_a(t)$ , defined as:

$$s_a(t) = s(t) + iH_s(t). \quad (3)$$

$s_a(t)$  is a complex signal from which it is possible to extract an instantaneous amplitude  $A(t)$  and an instantaneous phase  $\phi(t)$  so that  $s_a(t) = A(t)e^{i\phi(t)}$ .

### 3. Global behavior of the burner

As mentioned previously, the studied operating point is transient and corresponds to an increase of the equivalence ratio while maintaining the global flow rate constant. The evolution of the pressure fluctuations in the chamber during this transient operation is shown at the top of Fig. 2. At the beginning of the recording, the peak-to-peak pressure fluctuations are below 300 Pa while they reach almost 2000 Pa at the end. In the meantime, the power of the burner has only increased by around 7%, meaning that the increase in pressure fluctuations cannot only be related to the power increase.

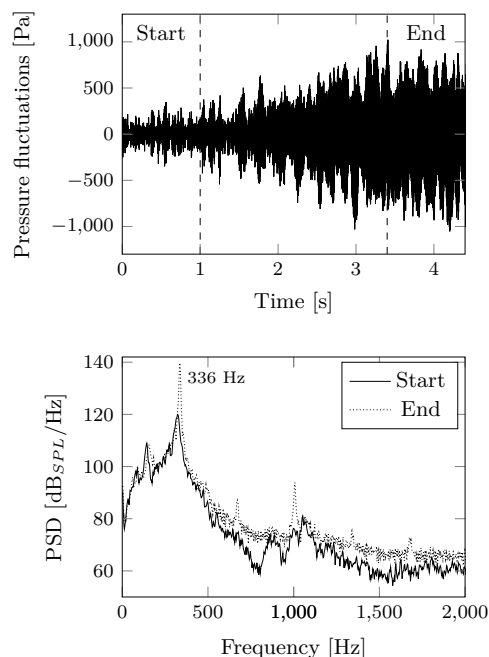


Figure 2: Top: Raw signal of the pressure fluctuations in the combustion chamber during the transient. Bottom: Spectra of the pressure fluctuations signal during the first and the last seconds of the recording.

The bottom of Fig. 2 shows spectra of the pressure signal during the first and last seconds of the recording. These power spectral density estimates are obtained using Welch's method, with 0.33 s long Hamming windows and 50% overlap. During the first second, the spectrum is characterized by a peak around 324 Hz, indicating moderate thermo-acoustic activity. The spectra for the end of the recording is globally the same as at the start, except for a strong peak at 336 Hz and its harmonics. This indicates that the strong increase in the pressure fluctuations amplitude is due to coherent fluctuations at this frequency, which corresponds to a strong thermo-acoustic instability. The increase in peak frequency between the start and the end of the recording can be explained by the increase in equivalence ratio which impacts the temperature in the combustion chamber. As the burnt gas temperatures increase, the speed of sound also increases and thus the resonant frequency for the instability follows the same trend.

To monitor major changes in the flame between the beginning and the end of the recording, average images are used. They are shown in Fig. 3 where only the right part of the burner is studied. The left part of the images are the mirror images of the right part of the burner

averaged during the first second and the right part corresponds to an averaging during the last second.

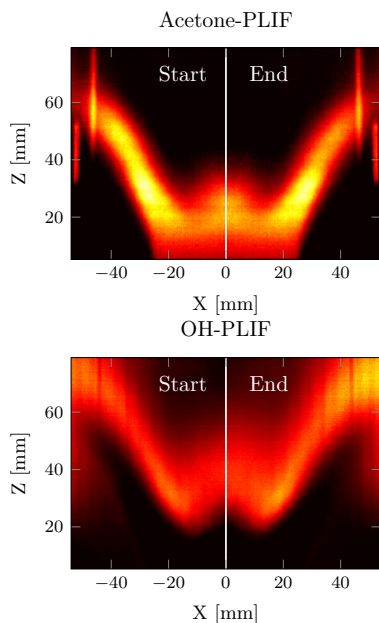


Figure 3: Average images of the right part of the burner taken during the first second (left) and the last second (right) of the recording. The vertical bars in the acetone images are due to laser reflections on the cylindrical chamber.

Whether from acetone-PLIF or OH-PLIF, the average images are similar between the beginning and the end of the recording meaning that no strong change to the flame stabilization occurs because of the change in equivalence ratio or the growth of the thermo-acoustic instability. In the acetone images, the only minor change comes from the top of the arm which shows lower levels than at the beginning of the recording. This tends to indicate that the fresh gases are burnt a bit earlier on average. This is confirmed by the OH images which show that the intensity at the top of the arm is higher in the end than in the beginning. The OH images also show higher levels in the burnt gases which is consistent with the equivalence ratio increase.

The dynamics of the PLIF recordings is studied thanks to a Dynamic Mode Decomposition of the data from the end of the recording, where the thermo-acoustic instability is the strongest. To combine multiple diagnostics, a stacked-DMD [22] procedure is used where the data from the OH-PLIF, acetone PLIF and pressure transducer are stacked into one matrix that is then processed by DMD. This way, the resulting dynamics come from the information of all diagnostics and the

phase reference is the same for all. Bins of  $4 \times 4$  pixels are used for the OH and acetone PLIF images and 10000 snapshots are used, corresponding to the last second of the recording. The DMD mode at 336 Hz is found to be dominating the others as expected and the parts of it corresponding to the OH and acetone PLIF are shown in Fig. 4. Since the temporal evolution of the mode corresponds only to a 336 Hz oscillation, all the interesting information can be found in the spatial parts that are shown in Fig. 4.

For the OH-PLIF image, the full field of view is shown on the left of Fig. 4. The dark regions indicate parts of the image where the signal does not fluctuate much with the combustion instability. They correspond to the fresh gases (no signal at all), the burnt gases region and the center part of the flame. This indicates that the thermo-acoustic instability influences almost only the arms of the flame and especially the tip of these arms. Another interesting feature is the symmetry of the image, indicating that two symmetrical parts of the flame fluctuate in phase and with comparable amplitude, as expected for a longitudinal thermo-acoustic instability.

Since the pressure signal is included in the stacked DMD, its phase in the common phase reference given by the DMD can be measured and is around  $\frac{\pi}{4}$ . This means that the pressure fluctuates in phase with the pink and blue parts of the images. This allows to estimate the Rayleigh index in this case by looking at the OH-PLIF image: the parts of the flame most contributing to the instability are at the top of the arms. This is consistent with other LSB studies reported in the literature [16].

The spatial shape of the acetone part of the stacked DMD mode is shown on the right of Fig. 4. As for the OH-PLIF results, some parts of the image are not fluctuating at all. These regions are the burnt gases (no acetone signal), the fresh gases and the center of the flame. The fluctuations mainly happen at the boundaries of the flame arm. An interesting feature is that, for a given position, the phase of the acetone fluctuations is opposite to the one of the OH fluctuations. This can easily be understood when one takes into account that acetone tracks the fresh gases and OH the burnt gases. Where there is a surge of fresh gases, there cannot be any burnt gases and conversely. Therefore, the acetone and OH signals can only have opposite behaviors.

Along the external part of the arm of the acetone image, it is possible to witness a continuous phase decrease in the downstream direction. This phase behavior is typical of the convection of the signal downstream. Indeed, by factoring in a sinusoidal temporal evolution, it is easy to see that such a phase evolution means that the

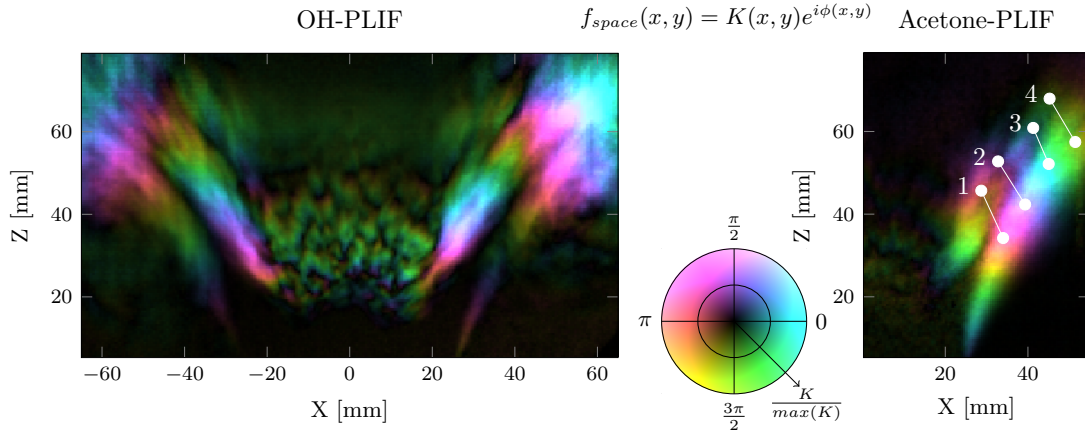


Figure 4: Spatial parts of the 336 Hz stacked DMD mode corresponding to the OH-PLIF (left) and acetone-PLIF (right) data. They are shown using a colormap that allows to represent both the modulus and angle of the complex quantity. The point couples shown in white are used for Fig. 6.

downstream parts reach a maximum with a delay that increases the further they are from the injector wall. The distance between two green parts in the image, such as (30 mm,20 mm) and (50 mm,55 mm) for example, can be estimated to 40 mm. Since they have the same phase, this means that the convection time between these two parts is one oscillation period at 336 Hz. This gives an estimation of the convection velocity of  $13 \text{ m}\cdot\text{s}^{-1}$  which is close to the expected flow velocity at these positions given that the bulk velocity is  $10 \text{ m}\cdot\text{s}^{-1}$  and that the velocity in the arms is higher [6]. This result is thus coherent with the findings of Therkelsen et al. [14] that indicate that the instability is linked with the convection of ring vortices from the burner rim.

To sum up, the images in Fig. 4, show that the thermo-acoustic instability is driven by the regular surge of fresh gases at the instability frequency. This excess of reactant is burnt as a burst at the top of the flame, creating a heat release there that is in phase with a higher pressure in the chamber, effectively giving energy to sustain the instability. In that sense, the instability mechanism in the flame arms is similar to what can be found in the literature for laminar premixed flames [23]. This however does not explain why such an instability is triggered when the equivalence ratio is increased. This is the main reason for the analysis carried out in the next section.

#### 4. Growth of the instability

Since it was shown that the OH and acetone-PLIF recordings are quite close, the present section focuses only on the acetone data and thus on the fresh gases dynamics. The acetone-PLIF field of view is divided into

$10\times 10$  pixels local averaging windows. The values of each of these windows then gives a set of 10 kHz signals that can be studied separately with classical signal processing tools. Each of these signals are divided into 1-second-long segments and the temporal average is removed so that only the fluctuating part remains. The power spectral density of each segment is estimated using Welch's method with 0.33 s long Hamming windows with 50% overlap. The peak frequency of each spectrum is then taken and its value is placed at the spatial position of the averaging window in the images shown in Fig. 5.

For most of the images, the peak frequency is below 200 Hz indicating that the acetone-PLIF signal is mostly fluctuating at low frequencies. In the beginning of the recording (below 2 seconds), the only part fluctuating around the thermo-acoustic frequency is the outer part of the fresh gases jet. However, closer to the end of the recording (that is, when the thermo-acoustic instability is stronger), it can be seen that the internal part is also fluctuating at 336 Hz. The images in Fig. 5 thus show that the growth of the thermo-acoustic instability is also associated with an evolution of the parts of the flame that react to it: while in the beginning, only the external part is fluctuating, the end shows that the whole arm is fluctuating.

To study the phase relationship between the internal and external parts of the arm, probe points couples are chosen and shown in Fig. 4. Each couple is made of one point in the external part of the arm and one in the internal part. The couples are chosen so that they have the two points have the same phase in the DMD result

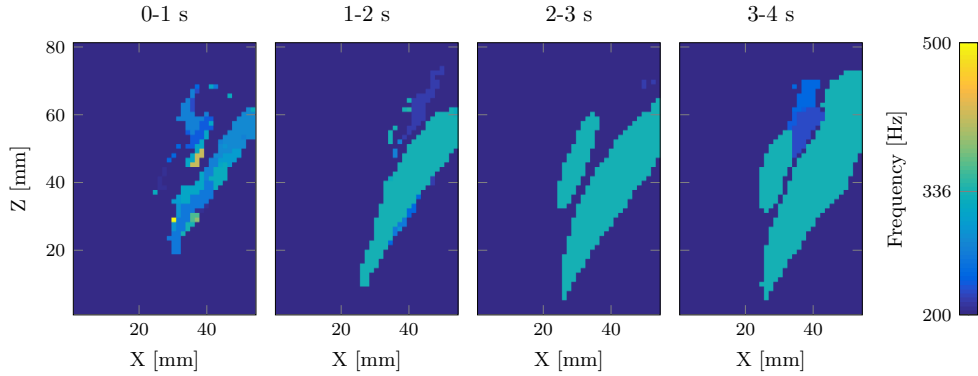


Figure 5: Maps of the peak frequency in the local spectra for four different 1-second-long segments of the acetone-PLIF recordings. The colormap is clipped below 200 Hz to focus on frequencies around the thermo-acoustic instability.

(*ie* at the end of the recording) and so that the four couples span one full instability cycle ( $\frac{\pi}{2}$  separation). The temporal signal from each of these points is bandpass filtered (center frequency: 336 Hz, bandwidth: 30 Hz) and its phase is computed by Hilbert transform. The phase difference associated with each couple can thus be obtained. Then, inside 0.1-second-long windows, the probability that the couple is in phase is computed by computing the ratio between the number of samples with a phase difference between  $-\frac{\pi}{2}$  and  $\frac{\pi}{2}$  and the total number of samples in the window. The evolution of this probability with time is given for the four couples in Fig. 6.

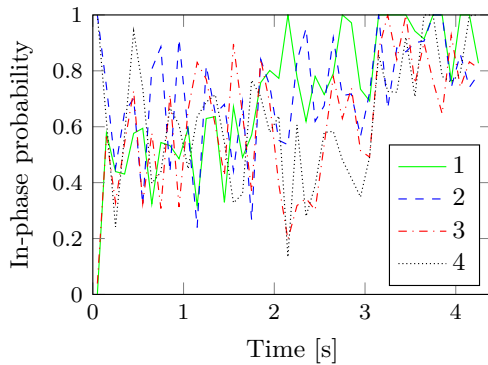


Figure 6: Probability that the point couples shown in Fig. 4 oscillate in phase as a function of time. Point couples from 1 to 4 go from the base of the flame arm to its extremity.

In the beginning, before the internal part of the arm starts to fluctuate at the thermo-acoustic frequency, it can be seen that the probability for all couples is around 0.5, corresponding to what is expected for two uncorrelated signals. However, as the internal part of the arm

starts to react, the in-phase probability of the couples increases until it is almost always above 0.7 at the end of the recording. This indicates that as soon as the internal part of the arm starts to fluctuate at the instability frequency (after 2 seconds, as shown in Fig.5), they are in phase with the external part and thus help to promote the bursts as both fluctuations then arrive at the same time at the top of the arm.

The growth of the instability due to the change in equivalence ratio happens therefore in two steps. First, the ring vortices detaching from the burner rim are acting on the external part of the flame. The timing of the flame burst they create around the top of the external parts of the flame arms is changed because the flame speed is increased by the increase in equivalence ratio which leads to an amplification of the pressure fluctuations. Then, the internal parts of the flame arms start to fluctuate in phase with the external parts and reinforce the bursting mechanism.

## 5. Conclusion

By increasing the equivalence ratio and keeping the bulk velocity in a low-swirl burner, the pressure fluctuations inside the combustion chamber are shown to tremendously increase even though the power change remains limited. This is due to the growth of a thermo-acoustic instability at 336 Hz. While this instability does not change the average flame shape or stabilization mechanism, it has a strong impact on the flame arm which starts to periodically release bursts of fresh gases. The subsequent bursts of flame are shown to happen in phase with the high part of the pressure fluctuation cycle, effectively adding energy to the oscillation. Originally generated by the convection of ring vortices de-

tached from the injector rim, the bursts are then amplified by the fact that the internal and external boundaries of the flame arm fluctuate in phase, which can be related to a change in flame speed.

This mechanism is inferred from the available time-resolved data processed with state of the art methods but would require further studies to be confirmed. For example, since the proposed mechanism is purely kinematic, a turbulent g-equation solver could help in studying it.

## Acknowledgments

We would like to thank Mr Kotaro Moriyama regarding the experimental work on which this study is based. The stay of Antoine Renaud at JAXA and Keio University has been supported by the Erasmus Mundus EASED program (Grant 2012-5538/004-001) coordinated by CentraleSupélec.

## References

- [1] A. H. Lefebvre, *Journal of Engineering for Gas Turbines and Power* 117 (4) (1995) 617–654.
- [2] S. Candel, *Proceedings of the Combustion Institute* 29 (1) (2002) 1–28.
- [3] C. K. Chan, K. S. Lau, W. K. Chin, R. K. Cheng, *Symposium (International) on Combustion* 24 (1) (1992) 511–518.
- [4] R. K. Cheng, *Combustion and Flame* 101 (1-2) (1995) 1–14.
- [5] W. Nazeer, K. Smith, P. Sheppard, R. Cheng, D. Littlejohn, *ASME*, 2006, pp. 107–115.
- [6] R. K. Cheng, D. Littlejohn, W. A. Nazeer, K. O. Smith, *Journal of Engineering for Gas Turbines and Power* 130 (2) (2008) 021501.
- [7] R. K. Cheng, D. Littlejohn, P. A. Strakey, T. Sidwell, *Proceedings of the Combustion Institute* 32 (2) (2009) 3001–3009.
- [8] D. Littlejohn, R. K. Cheng, D. R. Noble, T. Lieuwen, *Journal of Engineering for Gas Turbines and Power* 132 (1) (2010) 011502+.
- [9] P. Petersson, J. Olofsson, C. Brackman, H. Seyfried, J. Zetterberg, M. Richter, M. Aldén, M. A. Linne, R. K. Cheng, A. Nauert, Others, *Applied optics* 46 (19) (2007) 3928–3936.
- [10] D. M. Kang, F. E. C. Culick, A. Ratner, *Combustion and Flame* 151 (3) (2007) 412–425.
- [11] S. Tachibana, J. Yamashita, L. Zimmer, K. Suzuki, A. K. Hayashi, *Proceedings of the Combustion Institute* 32 (2) (2009) 1795–1802.
- [12] Y. Huang, A. Ratner, *Journal of Propulsion and Power* 25 (2) (2009) 365–373.
- [13] I. Yilmaz, A. Ratner, M. Ilbas, Y. Huang, *International Journal of Hydrogen Energy* 35 (1) (2010) 329–336.
- [14] P. L. Therkelsen, J. E. Portillo, D. Littlejohn, S. M. Martin, R. K. Cheng, *Combustion and Flame* 160 (2) (2013) 307–321.
- [15] M. Emadi, K. Kaufman, M. W. Burkhalter, T. Salameh, T. Gentry, A. Ratner, *International Journal of Hydrogen Energy* 40 (39) (2015) 13594–13603.
- [16] S. Tachibana, K. Kanai, S. Yoshida, K. Suzuki, T. Sato, *Proceedings of the Combustion Institute* 35 (3) (2015) 3299–3308.
- [17] K. Kohse-Höinghaus, R. S. Barlow, M. Aldén, J. Wolfrum, *Proceedings of the Combustion Institute* 30 (1) (2005) 89–123.
- [18] B. Böhm, C. Heeger, R. Gordon, A. Dreizler, *Flow, Turbulence and Combustion* 86 (3-4) (2011) 313–341.
- [19] C. T. Chong, S. Hochgreb, *Combustion and Flame* 158 (3) (2011) 490–500.
- [20] P. J. Schmid, *Journal of Fluid Mechanics* 656 (2010) 5–28.
- [21] P. J. Schmid, *Experiments in Fluids* 50 (4) (2011) 1123–1130.
- [22] F. Richecoeur, L. Hakim, A. Renaud, L. Zimmer, *Proceedings of the Summer Program* (2012) 459.
- [23] D. Durox, T. Schuller, S. Candel, *Proceedings of the Combustion Institute* 30 (2) (2005) 1717–1724.